

Graphene-based transparent flexible heat conductor for thermally tuning nanophotonic integrated devices

Longhai Yu, Daoxin Dai, and Sailing He

Citation: [Applied Physics Letters](#) **105**, 251104 (2014); doi: 10.1063/1.4905002

View online: <http://dx.doi.org/10.1063/1.4905002>

View Table of Contents: <http://scitation.aip.org/content/aip/journal/apl/105/25?ver=pdfcov>

Published by the [AIP Publishing](#)

Articles you may be interested in

[Hybrid graphene/silicon integrated optical isolators with photonic spin-orbit interaction](#)

Appl. Phys. Lett. **108**, 151103 (2016); 10.1063/1.4945715

[Rigorous calculation of nonlinear parameters in graphene-comprising waveguides](#)

J. Appl. Phys. **118**, 023105 (2015); 10.1063/1.4926501

[Buried anti resonant reflecting optical waveguide based on porous silicon material for an integrated Mach Zehnder structure](#)

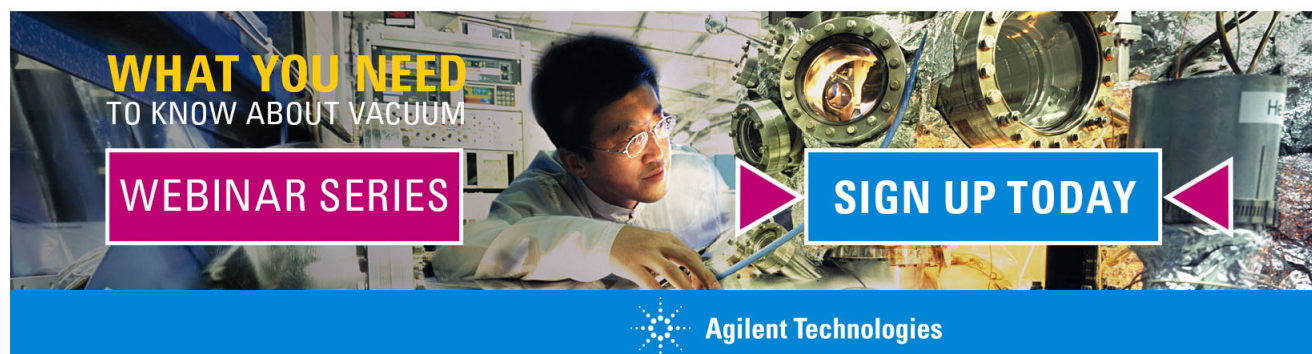
Appl. Phys. Lett. **101**, 191114 (2012); 10.1063/1.4766729

[Optical absorption in graphene integrated on silicon waveguides](#)

Appl. Phys. Lett. **101**, 111110 (2012); 10.1063/1.4752435

[Thermal trimming and tuning of hydrogenated amorphous silicon nanophotonic devices](#)

Appl. Phys. Lett. **97**, 071120 (2010); 10.1063/1.3479918

The advertisement features a background image of a man in a white lab coat working with a complex piece of scientific equipment. Overlaid on the image are several text elements: 'WHAT YOU NEED TO KNOW ABOUT VACUUM' in yellow and white, 'WEBINAR SERIES' in white on a pink rectangular background, and 'SIGN UP TODAY' in white on a blue rectangular background. Two pink arrowheads point towards the 'SIGN UP TODAY' button. At the bottom, the Agilent Technologies logo and name are displayed on a blue background.

WHAT YOU NEED
TO KNOW ABOUT VACUUM

WEBINAR SERIES

SIGN UP TODAY

Agilent Technologies

Graphene-based transparent flexible heat conductor for thermally tuning nanophotonic integrated devices

Longhai Yu,¹ Daoxin Dai,¹ and Sailing He^{1,2,a)}

¹Centre for Optical and Electromagnetic Research, Zhejiang Provincial Key Laboratory for Sensing Technologies, Zhejiang University, Hangzhou 310058, China

²Department of Electromagnetic Engineering, School of Electrical Engineering, Royal Institute of Technology, Stockholm S-100 44, Sweden

(Received 23 October 2014; accepted 12 December 2014; published online 24 December 2014)

Graphene, a well-known two-dimensional sheet, has attracted strong interest for both fundamental studies and applications. Due to its high intrinsic thermal conductivity, graphene has many potential applications in thermal management, such as in heat spreaders and flexible heaters. In this paper, a graphene-based transparent flexible heat conductor for nanophotonic integrated devices is demonstrated. The graphene heat conductor is designed to deliver heat from a non-local traditional metal heater to nanophotonic integrated devices for realizing efficient thermal tuning. With the present graphene heat conductor, a thermally tuning silicon Mach-Zehnder interferometer and micro-disk have been realized with good performance in terms of heating efficiency and temporal response. This indicates that the present graphene-based transparent flexible heat conductor provides an efficient and beneficial heating method for thermally tuning nanophotonic integrated devices. © 2014 AIP Publishing LLC. [<http://dx.doi.org/10.1063/1.4905002>]

Metal heaters have been widely used in large-scale photonic integrated circuits (PICs) to realize thermally tuning nanophotonic integrated devices, such as wavelength-tunable lasers,^{1,2} thermo-optical (TO) modulators,^{3,4} optical filters and switches,^{5,6} etc.⁷ However, it is challenging to utilize traditional metal heaters for some applications. For example, it is not convenient to utilize metal heaters on complex surfaces with non-planar nanostructures due to their poor flexibility. Moreover, in surface-emitting integrated devices (e.g., vertical-cavity surface-emitting lasers), metal heaters usually need to be designed carefully in order to avoid excess light absorption.¹ This will increase the fabrication complexity for metal heaters, especially in a nano-scale integrated device. Therefore, it is desired to have a heating method which can be easily used in all kinds of thermally tuning nanophotonic integrated devices.

Graphene has attracted strong interest for both fundamental studies and applications since the two-dimensional (2D) sheet was first exfoliated in 2004.⁸ Due to its unique structure, graphene has many extraordinary mechanical, electronic, and photonic properties, such as a thickness of 0.34 nm for a single layer of graphene, an absorption of $\sim 2.3\%$ per layer for vertically incident light, a carrier mobility as high as $200\,000\text{ cm}^2\text{ V}^{-1}\text{ s}^{-1}$ at room temperature, an electrochemically tunable Fermi level, a high optical damage threshold, and excellent mechanical stability.^{9–11} Graphene is also suggested to have exceptionally high intrinsic thermal conductivity of up to 5300 W/(m K) at room temperature,^{10,12} which results from the long-wavelength phonon transport in its 2D crystal lattices.^{13,14} Leveraging this property enables many potential applications of graphene in thermal management,^{15,16} such as

graphene heat spreaders in electronic and optoelectronic devices,^{17,18} high-performance transparent flexible graphene heaters,^{19,20} etc.^{21,22}

In this paper, we propose and demonstrate a graphene-based transparent flexible heat conductor for thermally tuning nanophotonic integrated devices. The graphene-based transparent flexible heat conductor is used to deliver heat from non-local metal heaters to a part of the nanophotonic integrated devices. Because of the single-atom thickness and the transparency of graphene, the proposed graphene heat conductor can be utilized in almost any substrate or platform, such as silicon and silica.^{23–25} Furthermore, the excellent flexibility of graphene makes it available for complex surfaces with non-planar nanostructures.²⁶ Therefore, the proposed graphene heat conductor is very convenient for various photonic integrated devices that need thermal management. Here, we present silicon-based thermally tuning Mach-Zehnder interferometers (MZIs) and micro-disk resonators with the graphene-based transparent flexible heat conductor. Both the simulation and experimental results show that the graphene heat conductor provides an effective approach for non-local heating.

Fig. 1(a) shows the three-dimensional structure of the thermally tuning silicon MZI with a graphene heat conductor. The silicon interferometer is fabricated on a commercial silicon-on-insulator (SOI) wafer with a 250 nm-thick top silicon layer and a 3 μm -thick buried oxide (BOX) layer by using the processes of electron beam lithography (EBL) and inductive coupling plasma (ICP) etching. The lengths of the two MZI arms are about $L_1 = 120\text{ }\mu\text{m}$, and $L_2 = (L_1 + 2\Delta L) = 180\text{ }\mu\text{m}$, respectively, as shown in the figure. Then a second EBL process and a lift-off process were carried out to make a 100 nm-thick titanium heater on top of the BOX layer (see Fig. 1(a)). As shown in Fig. 1(b), the width of the metal heater is about $w_m = 1.5\text{ }\mu\text{m}$, and the distance between the metal heater and the heated MZI arm is about $d_m = 4\text{ }\mu\text{m}$. A mono-layer

^{a)} Author to whom correspondence should be addressed. Electronic mail: sailing@kth.se.

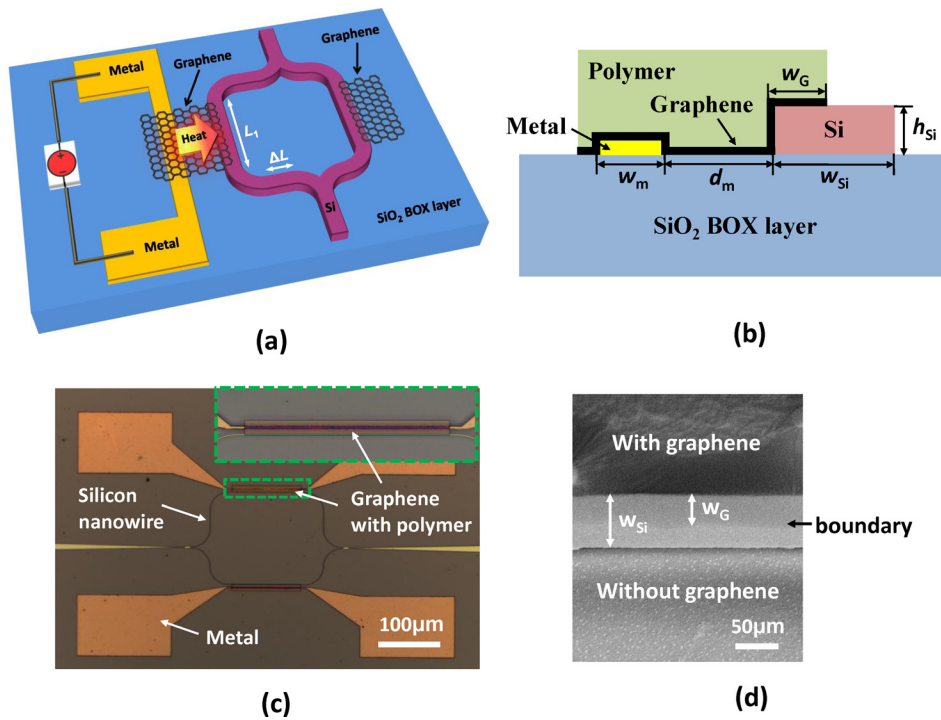


FIG. 1. (a) Three-dimensional schematic illustration of a thermally tuning MZI with a non-local traditional metal heater and a graphene-based transparent flexible heat conductor. Same graphene patterns are fabricated on both arms of the MZI. The polymer on the graphene is not shown. (b) Cross-section view for the heated MZI arm with a metal heater and a graphene heat conductor. (c) Top-view microscope image of the fabricated thermally tuning MZI (Scale bar: 100 μm). Inset, a zoom-in view for the heated MZI arm in the green dashed square. The graphene sheet is covered by a polymer film. (d) Top-view SEM image of the SOI nanowire covered by the patterned graphene sheet partly (Scale bar: 50 μm).

graphene sheet grown by chemical vapour deposition (CVD) is then wet-transferred onto the SOI chip and patterned by an oxygen plasma etching process to form the heat conductor.^{23,27} This graphene heat conductor covers the metal and a part of the heated MZI arm. The SOI nanowire is covered partially in the lateral direction to reduce the excess loss due to the graphene absorption (see Figs. 1(a) and 1(b)). Another identically patterned graphene sheet is also placed on the reference MZI arm in order to maintain balance, thus achieving a high extinction ratio.²⁴ In order to protect the patterned graphene from damage or contamination, the photoresist for patterning is not removed, as shown in Figs. 1(b) and 1(c). Since light is mainly confined to the silicon core region, the photoresist does not notably influence the thermal behavior of the devices (see below). Fig. 1(d) shows an SEM image of the SOI nanowire covered by the patterned graphene. It can be seen that the graphene sheet flexibly crosses the step from the BOX top surface to the top surface of the silicon core as desired.

The propagation losses of an SOI nanowire with a graphene heat conductor are mainly due to the absorption of graphene, and thus they are significantly dependent on the dimensions (w_{Si} , w_G) of the SOI nanowire and the graphene

on it (see Fig. 1(b)). A finite-element method (FEM) mode-solver is used to evaluate the propagation losses for TE and TM polarization modes, and the waveguide parameters are optimized to minimize the excess loss. Fig. 2(a) shows the calculated propagation losses for TE and TM polarization modes (see the inset of Fig. 2(a)) as the width w_G of graphene on the SOI nanowires varies when $w_{Si} = 500$ nm. With the increase of w_G , the propagation losses for both polarization modes increase. Therefore, it is desired to have a narrow graphene nano-ribbon on the SOI nanowires. Here, we choose $w_G = 300$ nm regarding the fabrication process. Then, we calculate the propagation losses for the case of $w_G = 300$ nm as the width w_{Si} of the SOI nanowire varies in Fig. 2(b). This shows that the propagation losses significantly decrease for both TE and TM polarization modes when w_{Si} increases from 400 nm to 600 nm. When $w_{Si} \sim 700$ nm, the propagation loss of the TM polarization mode has a kink (see Fig. 2(b)), which is from the mode hybridization. Regarding the single-mode condition, we choose $w_{Si} = 600$ nm. Moreover, it can be seen that the propagation loss for the TE polarization mode is much smaller than that for the TM polarization mode, so we choose to measure the TE polarization

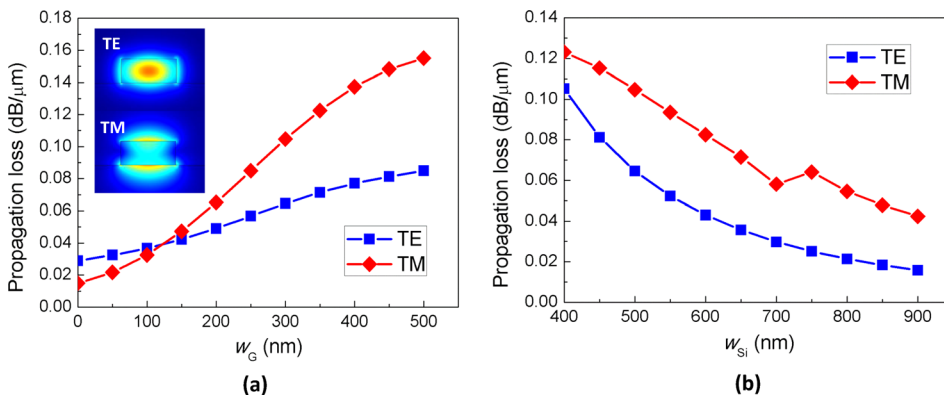


FIG. 2. (a) Propagation losses for TE and TM polarization modes as w_G varies when $w_{Si} = 500$ nm. Inset, TE (top) and TM (bottom) polarization modes of an SOI nanowire. (b) Propagation losses for TE and TM polarization modes as w_{Si} varies when $w_G = 300$ nm.

mode in the following experiments. The corresponding propagation loss is ~ 0.04 dB/ μm , which is much smaller than those of previous graphene-silicon hybrid SOI nanowires.^{23,24,27} A graphene transparent heat conductor is achieved.

It is well known that the output power P_{out} of the MZI can be described as²⁴

$$P_{\text{out}}(\lambda) = \frac{1}{2} P_{\text{in}} e^{-\alpha L_1} \left[1 + \cos \frac{2\pi}{\lambda} (n_e L_1 + 2n_{e0} \Delta L - n_{e0} L_1) \right], \quad (1)$$

where P_{in} is the input power, α is the attenuation coefficient of the graphene-covered SOI nanowire, n_e and n_{e0} are the effective refractive index of SOI-nanowire arms with and without heating, T and T_0 are the corresponding temperatures of the silicon core, respectively, and $T_0 = 300$ K is the room temperature with no heating. When the heating power is loaded in the metal heater, the graphene heat conductor will deliver heat from the metal heater to heat the corresponding MZI arm. When the temperature (T) increases for the SOI nanowire, its effective refractive index (n_e) increases due to the positive TO coefficient of silicon ($\sim 1.8 \times 10^{-4}/\text{K}$ at the wavelength of $1.55 \mu\text{m}$).⁵ As a consequence, a phase difference is introduced between the two arms, and the spectral response of the MZI has a redshift (see Eq. (1)). Regarding that the graphene heat conductor is also an electrical conductor, there is some current in the graphene sheet as well as the SOI nanowire covered with graphene when the current is injected for heating. Note that the estimated resistance of the graphene sheet in our case (with a sheet size of $\sim 4 \mu\text{m} \times 120 \mu\text{m}$) is as high as 10^4 – 10^5 ohms,^{9,28} which is much larger than that of the titanium heater in our device ($\sim 10^2 \Omega$). Therefore, the

electrically heating in the graphene sheet and the SOI nanowire is negligible as discussed above.

The dynamic spectral response of the fabricated thermally tuning MZI is also measured, as shown in Fig. 3(a). When the heating power P_{heating} varies from 0 mW to 110 mW, the spectral response has a redshift of ~ 7 nm. According to Eq. (1), we can calculate the corresponding temperature change $\Delta T = T - T_0$ for the heated SOI nanowire as shown in Fig. 3(b). It can be seen that the temperature change ΔT increases linearly with the heating power P_{heating} . The heating efficiency for the SOI nanowires, which is defined as the temperature change in unit volume under unit heating power, is calculated to be about $\eta = 7.61 \text{ K} \cdot \mu\text{m}^3/\text{mW}$. This value indicates the conversion efficiency from the electrical heating power to the temperature change of the SOI nanowire, which includes two processes, i.e., the heat generation in the metal heater and the heat delivery from the metal heater to the SOI nanowire.

Fig. 3(b) also shows the simulated temperature distribution in the region including the metal heater, the graphene heat conductor, and the SOI nanowire (see inset). Here, an FEM solver for the Poisson equation is used, where the graphene sheet is regarded as a 0.34 nm -thick layer with thermal conductivity of $\sim 2000 \text{ W}/(\text{m K})$.²⁹ (The thermal conductivity of the graphene, which is supported on the substrate in our case, is lower than that of a suspended graphene sheet.) The thermal conductivities of silicon, silica, and polymer are $\sim 80 \text{ W}/(\text{m K})$, $\sim 1.38 \text{ W}/(\text{m K})$, and $\sim 0.19 \text{ W}/(\text{m K})$, respectively, and the heat convection coefficient of air is set to $\sim 5 \text{ W}/(\text{m}^2 \text{ K})$.³⁰ In the simulation, it is assumed that the electrical energy for heating is converted completely to thermal energy. The result shows that the temperature distribution is not symmetric around the metal heater. The heat delivery is

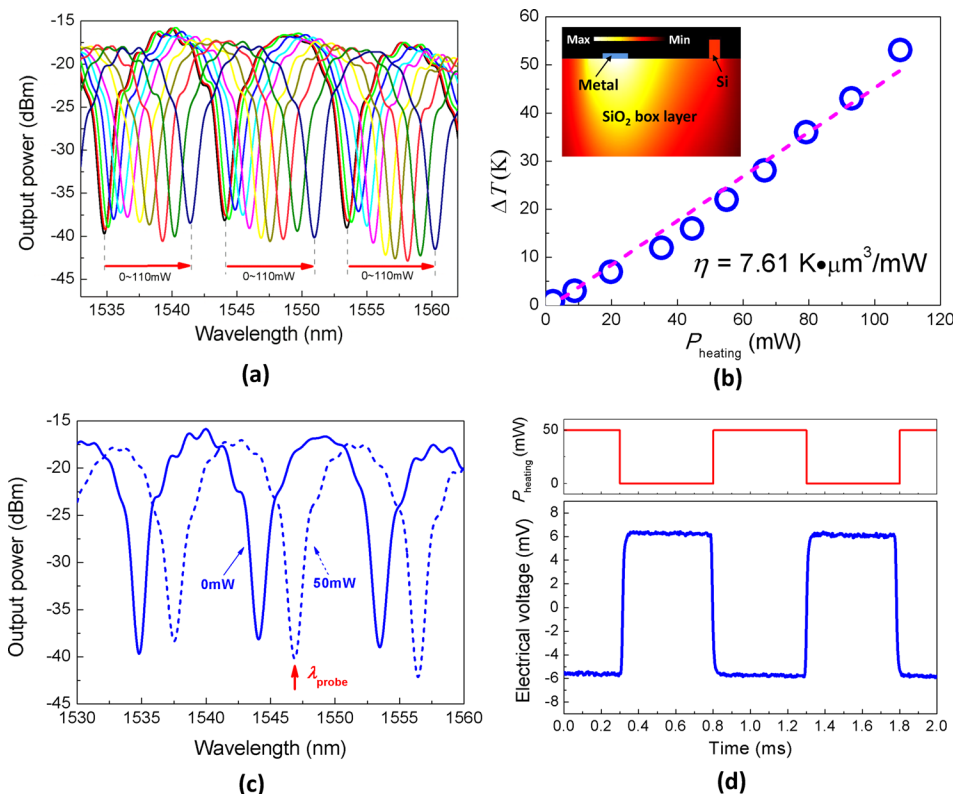


FIG. 3. (a) Spectral responses of the thermally tuning MZI as the heating power P_{heating} varies from 0 mW to 110 mW. (b) Temperature change ΔT for the core of the SOI nanowire with varying heating powers. The heating efficiency is about $\eta = 7.61 \text{ K} \cdot \mu\text{m}^3/\text{mW}$. Inset, normalized temperature distribution of a heated SOI nanowire simulated by using the Poisson equation with an FEM tool. The metal heater is shown in a blue line. The polymer on the graphene is not shown here since it will not significantly influence the thermal behaviors. (c) Spectral responses of the thermally tuning MZI when P_{heating} is 0 mW (solid line) and 50 mW (dashed line). The probe wavelength for the measurement of temporal responses is indicated. (d) Temporal responses for the modulated heating power P_{heating} (up) and the corresponding output of the thermally tuning MZI (down). The modulation frequency is 1 kHz.

enhanced on the right side of the heater because of the excellent heat conductivity of the graphene heat conductor. The simulated heating efficiency is about $\sim 8.53 \text{ K } \mu\text{m}^3/\text{mW}$, which is slightly higher than the measurement result. This mainly results from the quality degradation of the graphene sheet during the fabrication process. In our experiment, we observed that the wet-transferred graphene sheet has some contamination and cracks, which declines the heat conductivity of graphene. Another reason is that the conversion efficiency from the electrical energy for heating to thermal energy can never be ideally 100%. As indicated in the inset of Fig. 3(b), the heat can also be delivered from the metal heater to the SOI nanowire through the SiO_2 BOX layer. However, the simulation shows that the heating efficiency without the graphene heat conductor is only half of that with the graphene heat conductor in our case. From the simulation, we can also get the heating efficiency without the photoresist on the graphene, and the value is $\sim 8.20 \text{ K } \mu\text{m}^3/\text{mW}$, which is very close to that with the photoresist in our case. Therefore, the polymer on the graphene sheet does not influence the heating efficiency of the device as desired, which is due to its poor heat conductivity.

To study the temporal response of the thermally tuning MZI, the electrical power for heating is modulated with an amplitude of 50 mW, and the probe light is fixed at the wavelength $\lambda_{\text{probe}} = 1547 \text{ nm}$. As shown in Fig. 3(c), there is a maximal transmission at the probe wavelength when $P_{\text{heating}} = 0 \text{ mW}$ (see the solid line), while the transmission becomes minimal when the electrical power $P_{\text{heating}} = 50 \text{ mW}$ because of the thermal-optical redshift. In this way, the probe light is modulated, and this modulated output light is received by a photo-detector in our experimental setup. The corresponding output signal is shown in Fig. 3(d) when the modulation frequency of the heating power is about 1 kHz. In the figure, we can find that the 90% rising and decaying times (defined as the time it takes for the change in temperature to reach 90% of the maximum value from zero) are $\sim 20 \mu\text{s}$. We also simulate the temporal response by using the FEM tool, and the calculated rising and decaying times are about $16 \mu\text{s}$, which is slightly faster than the measurement result.

As one of graphene's advantages is its ability to be easily patterned into a nano-scale size with a CMOS-compatible fabrication process,^{31,32} the present graphene transparent flexible heat conductor can be applied conveniently to heat

extremely small thermally tuning devices, for which the conventional metal heater might be too large to fit the device size. For example, an extremely small thermally tuning silicon micro-disk resonator is designed and fabricated with a graphene heat conductor. In this example, the radius of the micro-disk resonator is chosen to be $R = 5 \mu\text{m}$ (though it is possible to be smaller), and the fabrication process of the device is the same as that for the thermally tuning MZI demonstrated above. The graphene heat conductor covers a part of the micro-disk to reduce excess loss, as shown in the inset of Fig. 4(a). The dynamic spectral responses of the micro-disk are measured and shown in Fig. 4(a), from which it can be seen that the resonant wavelength of the micro-disk has a redshift of $\sim 1 \text{ nm}$ when the heating power P_{heating} varies from 0 mW to 38 mW. As is known, the spectral response of the micro-disk is calculated as³³

$$P_{\text{out}}(\lambda) = P_{\text{in}} \left[\frac{t - e^{-i2\pi R \left(\frac{2\pi n_{\text{ed}}}{\lambda} - \alpha_d \right)}}{1 - t e^{-i2\pi R \left(\frac{2\pi n_{\text{ed}}}{\lambda} - \alpha_d \right)}} \right]^2, \quad (2)$$

where t is the transmission ratio in the coupling region of the micro-disk, α_d is the attenuation coefficient, and n_{ed} is the effective index of the gallery-whispering mode (GWM). From the temperature dependence of the effective index n_{ed} and the measured wavelength redshift of the spectral responses, the temperature change ΔT for the heated micro-disk can be estimated. From the result shown in Fig. 4(b), it can be seen that the temperature change ΔT increases linearly with the heating power P_{heating} , which is similar to that in the thermally tuning MZI. The heating efficiency for the $5 \mu\text{m}$ -radius micro-disk can be also derived as $\eta_d = 4.32 \text{ K } \mu\text{m}^3/\text{mW}$.

The experimental results for the thermal tuning in the silicon MZI and micro-disk demonstrated above show that the present graphene heat conductor provides an efficient heating approach for photonic integrated devices. We also note that the heating efficiency and temporal response can be enhanced with great potential. First, the graphene quality and its heat conductivity can be further improved by optimizing the fabrication process. The heating efficiency is calculated to be $\eta \sim 11.6 \text{ K } \mu\text{m}^3/\text{mW}$ when the thermal conductivity of graphene is increased to about $5000 \text{ W}/(\text{mK})$.^{12,29} Second, the metal heater can be placed closer to the heated SOI-nanowire waveguide so that the size of the graphene heat conductor is shrunk to reduce the heat spreading during the delivery in the graphene sheet. For example, when the distance d_m is reduced

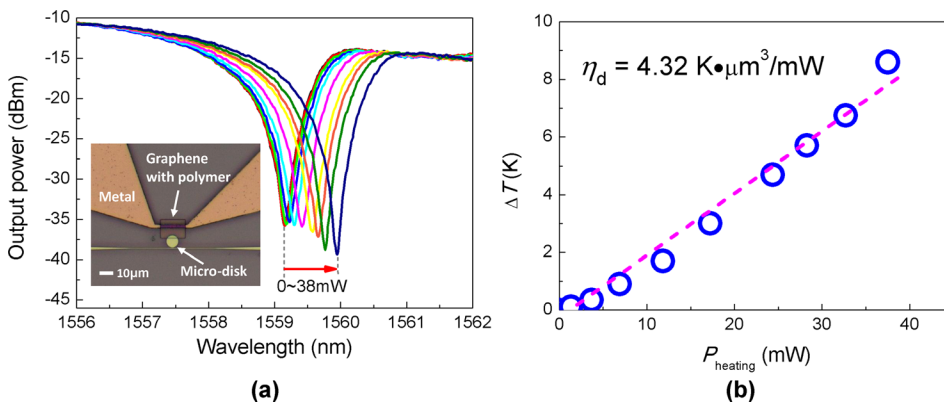


FIG. 4. (a) Spectral responses of the thermally tuning micro-disk as the heating power P_{heating} varies from 0 mW to 38 mW. Inset, top-view microscopy image of the fabricated thermally tuning micro-disk (scale bar: $10 \mu\text{m}$). (b) Temperature change ΔT for the silicon micro-disk with varying heating powers. The effective heating efficiency is about $\eta_d = 4.32 \text{ K } \mu\text{m}^3/\text{mW}$.

from $4\text{ }\mu\text{m}$ to $1\text{ }\mu\text{m}$, the simulation shows that the heating efficiency can be increased by more than four times (i.e., $\eta \sim 35.5\text{ K }\mu\text{m}^3/\text{mW}$) and the 90% rising and decaying times can be shortened to $\sim 9\text{ }\mu\text{s}$. Third, the thick SiO_2 BOX layer is such a large heat sink that it limits the heating efficiency and temporal response significantly, especially when the graphene heat conductor contacts the SiO_2 BOX layer in our case (see the inset of Fig. 3(b)). To overcome this problem, one can suspend the graphene sheet¹² or insert a layer with low heat conductivity (e.g., polymer) between the graphene sheet and the substrate to prevent the substrate heat from dissipating.

In summary, a graphene transparent flexible heat conductor that can achieve non-local heating for thermally tuning photonic integrated devices has been demonstrated. Thermally tuning MZIs and micro-disks have been realized with the present graphene transparent flexible heat conductor. For these devices, the graphene sheet partially covers the metal heater and the SOI nanowire to be heated so that the heat energy can be delivered. It has been shown that the excellent heat conductivity, transparency, and flexibility of graphene make it attractive as a heat conductor for thermally tuning devices, particularly when the metal heater cannot be applied in the traditional way. The heat efficiency and the temporal response can be further improved with optimized designs and fabrication processes.

This work was partially supported by the National Natural Science Foundation of China (Nos. 91233208 and 61422510), the National High Technology Research and Development Program (863) of China (No. 2012AA012201), and the Program of Zhejiang Leading Team of Science and Technology Innovation. This work was also supported by the Swedish VR grant (No. 621-2011-4620), and SOARD.

- ¹S. S. Yang, J. K. Son, Y. K. Hong, Y. H. Song, H. J. Jang, S. J. Bae, Y. H. Lee, G. M. Yang, H. S. Ko, and G. Y. Sung, *IEEE Photonics Technol. Lett.* **20**(17–20), 1679 (2008).
- ²Y. Uchiyama, T. Kondo, K. Takeda, A. Matsutani, T. Uchida, T. Miyamoto, and F. I. Koyama, *IEEE LEOS Annu. Meet.* **2005**, 326.
- ³W. S. Fegadolli, V. R. Almeida, and J. E. B. Oliveira, *Opt. Express* **19**(13), 12727 (2011).
- ⁴W. S. Fegadolli, L. Feng, M. Mujeeb-U-Rahman, J. E. B. Oliveira, V. R. Almeida, and A. Scherer, *Opt. Express* **22**(3), 3425 (2014).
- ⁵R. L. Espinola, M. C. Tsai, J. T. Yardley, and R. M. Osgood, *IEEE Photonics Technol. Lett.* **15**(10), 1366 (2003).
- ⁶J. E. Cunningham, I. Shubin, X. Z. Zheng, T. Pinguet, A. Mekis, Y. Luo, H. Thacker, G. L. Li, J. Yao, K. Raj, and A. V. Krishnamoorthy, *Opt. Express* **18**(18), 19055 (2010).

- ⁷Y. O. Noh, C. H. Lee, J. M. Kim, W. Y. Hwang, Y. H. Won, H. J. Lee, S. G. Han, and M. C. Oh, *Opt. Commun.* **242**(4–6), 533 (2004).
- ⁸K. S. Novoselov, A. K. Geim, S. V. Morozov, D. Jiang, Y. Zhang, S. V. Dubonos, I. V. Grigorieva, and A. A. Firsov, *Science* **306**(5696), 666 (2004).
- ⁹F. Bonaccorso, Z. Sun, T. Hasan, and A. C. Ferrari, *Nat. Photonics* **4**(9), 611 (2010).
- ¹⁰Q. L. Bao and K. P. Loh, *ACS Nano* **6**(5), 3677 (2012).
- ¹¹A. Vakil and N. Engheta, *Science* **332**(6035), 1291 (2011).
- ¹²A. A. Balandin, S. Ghosh, W. Z. Bao, I. Calizo, D. Teweldebrhan, F. Miao, and C. N. Lau, *Nano Lett.* **8**(3), 902 (2008).
- ¹³A. A. Balandin, *Nat. Mater.* **10**(8), 569 (2011).
- ¹⁴D. L. Nika, E. P. Pokatilov, A. S. Askerov, and A. A. Balandin, *Phys. Rev. B* **79**(15), 155413 (2009).
- ¹⁵M. M. Sadeghi, M. T. Pettes, and L. Shi, *Solid State Commun.* **152**(15), 1321 (2012).
- ¹⁶S. Ghosh, I. Calizo, D. Teweldebrhan, E. P. Pokatilov, D. L. Nika, A. A. Balandin, W. Bao, F. Miao, and C. N. Lau, *Appl. Phys. Lett.* **92**(15), 151911 (2008).
- ¹⁷S. Subrina, D. Khotchetkov, and A. A. Balandin, *IEEE Electron Device Lett.* **30**(12), 1281 (2009).
- ¹⁸R. Prasher, *Science* **328**(5975), 185 (2010).
- ¹⁹J. Kang, H. Kim, K. S. Kim, S. K. Lee, S. Bae, J. H. Ahn, Y. J. Kim, J. B. Choi, and B. H. Hong, *Nano Lett.* **11**(12), 5154 (2011).
- ²⁰D. Sui, Y. Huang, L. Huang, J. J. Liang, Y. F. Ma, and Y. S. Chen, *Small* **7**(22), 3186 (2011).
- ²¹N. Yang, G. Zhang, and B. W. Li, *Appl. Phys. Lett.* **95**(3), 033107 (2009).
- ²²S. D. Park, S. W. Lee, S. Kang, I. C. Bang, J. H. Kim, H. S. Shin, D. W. Lee, and D. W. Lee, *Appl. Phys. Lett.* **97**(2), 023103 (2010).
- ²³L. H. Yu, Y. Xu, Y. C. Shi, and D. X. Dai, in Proceedings of the Asia Communications and Photonics Conference, Guangzhou, China, 7–10 November 2012, AS1B.3.
- ²⁴H. Li, Y. Anugrah, S. J. Koester, and M. Li, *Appl. Phys. Lett.* **101**(11), 111110 (2012).
- ²⁵A. V. Babichev, H. Zhang, P. Lavenus, F. H. Julien, A. Y. Egorov, Y. T. Lin, L. W. Tu, and M. Tchernycheva, *Appl. Phys. Lett.* **103**(20), 201103 (2013).
- ²⁶Y. H. Kim, S. H. Kwon, J. M. Lee, M. S. Hwang, J. H. Kang, W. I. Park, and H. G. Park, *Nat. Commun.* **3**, 1123 (2012).
- ²⁷L. H. Yu, J. J. Zheng, Y. Xu, D. X. Dai, and S. L. He, *ACS Nano* **8**, 11386 (2014).
- ²⁸J. T. Smith, A. D. Franklin, D. B. Farmer, and C. D. Dimitrakopoulos, *ACS Nano* **7**(4), 3661 (2013).
- ²⁹A. N. Sidorov, D. K. Benjamin, and C. Foy, *Appl. Phys. Lett.* **103**(24), 243103 (2013).
- ³⁰L. Yang, D. X. Dai, and S. L. He, *Opt. Commun.* **281**(9), 2467 (2008).
- ³¹C. Berger, Z. M. Song, X. B. Li, X. S. Wu, N. Brown, C. Naud, D. Mayou, T. B. Li, J. Hass, A. N. Marchenkov, E. H. Conrad, P. N. First, and W. A. de Heer, *Science* **312**(5777), 1191 (2006).
- ³²A. Sinitskii and J. M. Tour, *Appl. Phys. Lett.* **100**(10), 103106 (2012).
- ³³W. Bogaerts, P. De Heyn, T. Van Vaerenbergh, K. De Vos, S. K. Selvaraja, T. Claes, P. Dumon, P. Bienstman, D. Van Thourhout, and R. Baets, *Laser Photonics Rev.* **6**(1), 47 (2012).